Global Minimum for Curvature Penalized Minimal Path Method

Da CHEN
chenda@ceremade.dauphine.fr
Jean-Marie MIREBEAU
mirebeau@ceremade.dauphine.fr
Lauren D. COHEN
cohen@ceremade.dauphine.fr

Université Paris Dauphine,
CNRS, CEREMADE, UMR7534
F-75016, Paris, France

Abstract

Minimal path or geodesic methods have been widely applied to image analysis and medical imaging [13]. However, traditional minimal path methods do not consider the effect of the curvature. In this paper, we propose a novel curvature penalized minimal path approach implemented via the anisotropic fast marching method and asymmetric Finsler metrics. We study the weighted Euler's elastica based geodesic energy and give an approximation to this energy by an orientation-lifted Finsler metric so that the proposed model can achieve a global minimum of this geodesic energy between the endpoint and initial source point. We also introduce a method to simplify the initialization of the proposed model. Experiments show that the proposed curvature penalized minimal path model owns several advantages comparing to the existed state-of-the-art minimal path models without curvature penalty both on synthetic and real images.

1 Introduction

The classical snake model [9] for boundary integration and curve extraction was proposed by Kass *et al*. A snake is a parametrized curve $\mathcal{C}$ (locally) minimizing the energy functional:

$$E_{snake}(\mathcal{C}) = \int_0^1 w_1 \|\mathcal{C}'(t)\|^2 + w_2 \|\mathcal{C}''(t)\|^2 + \mathcal{P}(\mathcal{C}(t))\, dt, \tag{1}$$

with appropriate boundary conditions at the endpoints $t = 0, 1$. Parameters w_1 and w_2 relate to the elasticity of and rigidity of the curve $\mathcal{C}$, hence weight its internal forces. Importantly, the second derivative $\|\mathcal{C}''(t)\|$ penalization amounts to a prior of *low curvature*. Potential function $\mathcal{P}$ attracts the curve to image features, where by design it takes the lowest values. Thus the active contour $\mathcal{C}$ is under control of the internal forces and image force. In [6, 7], the authors added an extra balloon inflation force allowing a less demanding initialization and in [24], the authors proposed a gradient vector field to control the curve evolution. The main practical drawback of the snake model is that the curve optimization procedure is often stuck at local minima of the energy functional, which makes results sensitive to curve initialization.

Pages 86.1-86.12
DOI: https://dx.doi.org/10.5244/C.29.86

Cohen and Kimmel proposed in [8] a geodesic or minimal path model, based on the energy functional:

$$E_{geo}(\mathcal{C}) = \int_0^1 (w + \mathcal{P}(\mathcal{C}(t)))\|\mathcal{C}'(t)\|\,dt. \tag{2}$$

In contrast with classical snake energy (1), this first order model does not penalize the second derivative of the curve $\mathcal{C}$, despite the relevance of curvature for the applications. Thanks to this simplification, a fast, reliable and globally optimal numerical method allows to find the energy minimizing curve with prescribed endpoints; namely the fast marching algorithm [20], based on the formalism of viscosity solutions to Eikonal Partial Differential Equations (PDE). These mathematical and algorithmic guarantees have important practical consequences, which allowed to deeply apply the minimal path model (2) and its extensions to image analysis and medical imaging [18]. Li and Yezzi [12] proposed a radius-lifted minimal path technique to extract the tubular boundaries and centrelines simultaneously. Péchaud *et al*. [17] proposed an orientation and radius-lifted isotropic minimal path, embedding the orientation information to the geodesic energy. All the mentioned methods above are isotropic minimal path techniques, in which the potential $\mathcal{P}$ depends only on the positions. Benmansour and Cohen [4] proposed an anisotropic radius-lifted minimal path model in which the potential $\mathcal{P}$ depends not only the positions but also the tangential directions $\mathcal{C}'$. This approach solves the *shortcut* problem that happens with the classical isotropic minimal path model. Chen *et al*. [9] proposed a region constrained minimal path model by assuming that the geodesic should be included completely inside the constrained region, to overcome the *overlapping extraction* problem. The keypoints method is a variant minimal paths method [7] which will automatically add initial source points during the fast marching front propagation and may easily apply to find a closed contour with only one given point. Some authors [5, 10] improved this keypoints minimal path method with automatic stopping criteria for open curves extraction.

Bekkers *et al*. [1] introduced a new geodesic model based on a sub-Riemannian metric and PDE approach which is related to curvature regularization. Graph based curvature-penalty models are well studied. Schoenemann *et al*. [19] proposed a curvature based globally optimal segmentation method by an extended graph representation and minimum ratio cycles. Strandmark *et al*. [22] introduce a shortest path model with curvature and torsion, in which the curve can be approximated by B-Splines. The path energy then can be minimized by Dijkstra's algorithm.

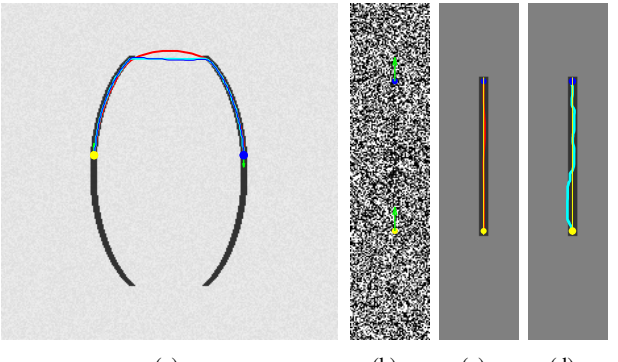

(a) (b) (c) (d)

Figure 1: Extraction results from different methods (see text).

Motivation of using curvature penalty: minimal path methods are first order models (2), which do not penalize second order derivatives, i.e. the curvature, and therefore do not enforce the smoothness of the minimizing curve $\mathcal{C}$. Hence those models cannot get good results when extracting curves with gaps and high noise. The model chosen in this paper reintroduces curvature, in the form of weighted Euler elastica's as studied by Mumford [16]. An adequate numerical implementation, leveraging orientation lifting, asymmetric Finsler metrics and anisotropic fast marching, still allows to find the globally minimizing curves with prescribed endpoints and tangents. We compare our model (red lines) with the classical minimal path [8] (cyan lines) and orientation-lifted minimal path [17] (blue lines) in Fig. 1. The yellow dots are the initial positions and blue dots are the end positions. In Fig. 1(a), we show the extraction results for a curvilinear structure with a big gap. Our model (red) smoothly completes the structure, in contrast with the straight line completion with broken angles of alternatives. Fig. 1(b) is an image with high noise, (c) is the result overlapped on the clean original image from the proposed model and (d) is the result using [8], while the yellow line indicates the groundtruth centreline. Curvature penalty thus allows both the completion of large gaps in structures, and the resilience to high noises.

The paper is organized as follows: in Section 2, we briefly introduce the existing minimal path methods and the state-of-the-art anisotropic fast marching method with arbitrary Finsler metric. We define Euler's elastica geodesic energy in Section 3 and orientation-lifted potential computation in Section 4. Numerical experiments are presented in Section 5.

2 Background

2.1 Minimal path model

The minimal path problem [18] is posed on a bounded domain Ω, and a metric $\mathcal{F}$ prescribing norm $\mathcal{F}_x$ (potentially asymmetric) at each point $x \in \Omega$. We denote by $\mathfrak{I}$ the collection of Lipschitz paths $\gamma : [0,1] \to \Omega$, and we measure path length through the metric $\mathcal{F}$:

$$l_{\mathcal{F}}(\gamma) = \int_0^1 \mathcal{F}_{\gamma(t)}(\dot{\gamma}(t))\, dt, \tag{3}$$

where $\dot{\gamma}(t) = \frac{d}{dt}\gamma(t)$. The geodesic distance $\mathcal{U}(x)$ from a set of initial source points $\mathcal{W}$, is the minimal energy of any path joining $x \in \Omega$ to $\mathcal{W}$:

$$\mathcal{U}(x) := \min\{l_{\mathcal{F}}(\gamma);\ \gamma \in \mathfrak{I},\ \gamma(1) = x,\ \gamma(0) \in \mathcal{W}\}. \tag{4}$$

The function $\mathcal{U}$, called the minimal action map, is the unique viscosity solution to an Eikonal PDE, defined in terms of the dual metric $\mathcal{F}^*$. For all $x \in \Omega$ one has $\mathcal{U}(x) = 0$ if $x \in \mathcal{W}$ and otherwise

$$\mathcal{F}^*_x(-\nabla \mathcal{U}(x)) = 1, \qquad \text{where } \mathcal{F}^*_x(u) = \sup_{v \neq 0} \frac{\langle u, v\rangle}{\mathcal{F}_x(v)}. \tag{5}$$

The metrics $\mathcal{F}$ considered in this paper combine a symmetric part, defined in terms of a symmetric positive tensor field $\mathcal{M}$, and an asymmetric part involving a vector field ω:

$$\mathcal{F}_x(u) := \sqrt{\langle u, \mathcal{M}(x)u\rangle} - \langle \omega(x), u\rangle. \tag{6}$$

We require $\langle \omega(x), \mathcal{M}(x)^{-1}\omega(x)\rangle < 1$ to ensure the metric positivity. Equation (6) defines a Finsler metric in general, an anisotropic Riemannian metric if the vector field ω is identically

zero, and an *isotropic* metric if in addition the tensor field $\mathcal{M}$ is everywhere diagonal. The fast marching method [20] solves the Eikonal PDE in the isotropic case. Efficient adaptations to Riemannian and Finsler metrics are presented in [14] and [15] respectively.

Isotropic Case: if the tensor field is proportional to the identity matrix $\mathcal{M}(x) = (w+\mathcal{P}(x))^2\mathbf{I}_d$, and if $\omega = 0$, then (3) becomes (2) the classical minimal path model [8] proposed by Cohen and Kimmel.

The image domain Ω can be extended by product with abstract parameter spaces: $\overline{\Omega} = \Omega \times S^1 \times \mathcal{R}^1$, typically accounting for the orientation $\theta \in S^1$, or radius $r \in \mathcal{R}^1 = [r_{\min}, r_{\max}]$ of tubular structures present in the processed image. A lifted path $\gamma = (\Gamma, \theta, r)$ has the length

$$l(\gamma) = \int_0^1 \mathcal{P}(\gamma(t)) \sqrt{\|\dot{\Gamma}(t)\|^2 + \varepsilon|\dot{\theta}(t)|^2 + \zeta|\dot{r}(t)|^2}\, dt, \tag{7}$$

corresponding (6) to the diagonal tensor field $\mathcal{M}(x)$ of entries $\mathcal{P}(x)^2(1,1,\varepsilon,\zeta)$. Li and Yezzi [12] introduced the radii based model ($\varepsilon = 0$) and used it to extract tubular structure centrelines and boundaries at the same time. Orientation lifting ($\varepsilon \neq 0$) often improves the results [17], but suffers from the fact that nothing in (7) constrains the path direction $\dot{\Gamma}$ to align with the tubular structure orientation θ, a point which is addressed in this paper.

Anisotropic Riemannian case: non diagonal tensor fields $\mathcal{M}$ improve on isotropic minimal path techniques by facilitating path propagation in specific directions, such as tangentially to tubular structures present in the processed image [4, 5].

Finsler case: active contours based on Finsler measures of path length are applied in [13] to image segmentation. Our approach differs by the choice of Finsler metric, the connection with Euler elastica's, and the use of a fast marching method for the Eikonal PDE instead of the less efficient sweeping method.

2.2 Anisotropic Fast Marching Method with Arbitrary Finsler Metric

To solve the problem presented in (4) in the general case of an arbitrary Finsler asymmetric metric $\mathcal{F}$, a new fast marching method using anisotropic stencil refinement (FM-ASR) was introduced by Mirebeau [15].

Numerical methods to compute the minimal action map $\mathcal{U}$, see (4), introduce a discretization grid Z of image domain Ω or extended domain $\overline{\Omega}$, and for each $x \in Z$ a small mesh $S(x)$ of a neighbourhood of x with vertices in Z. An approximation of $\mathcal{U}$ is given by the solution of the following fixed point problem: find $\mathcal{U} : Z \to \mathbb{R}$ such that (i) $\mathcal{U}(x) = 0$ for all initial points $x \in \mathcal{W}$, and (ii) for all $x \in Z \setminus \mathcal{W}$:

$$\mathcal{U}(x) = \min_{y \in \partial S(x)} \mathcal{F}_x(y-x) + \mathrm{I}_{S(x)}\mathcal{U}(y), \tag{8}$$

where I_S denotes piecewise linear interpolation on a mesh S. The expression (8) reflects the fact that the minimal path $\gamma_{x,\mathcal{W}}$, joining x to $\mathcal{W}$, needs to cross the stencil boundary $\partial S(x)$ at least once at some point y; hence it is the concatenation of a small path joining x to y, of approximate length $\mathcal{F}_x(y-x)$, and of γ_y, which energy is approximated by interpolation. A striking fact is that this N-dimensional fixed point system, with $N = \#(Z)$, can be solved in a single pass using the Fast Marching algorithm [23], provided the stencils $S(x)$ satisfy some geometric properties depending on the local Finsler metric $\mathcal{F}_x(\cdot)$. An adaptive construction of such stencils was introduced in [14, 15], which led to breakthrough improvements in terms of computation time and accuracy for strongly anisotropic geodesic energy metrics, as in our application. It relies on anisotropic stencil refinement, which combines in an optimal way

the geometric structure given by the asymmetric Finsler metric, and the arithmetic structure of the cartesian discretization grid.

3 Curvature Penalized Minimal Path model

Euler's Elastica bending Energy: Following Mumford [16], we consider weighted Euler elasticas, minimizing the following bending energy:

$$\mathcal{L}(\Gamma) = \int_0^L \Big(\frac{1}{\alpha(s)} + \frac{1}{\beta(s)}\kappa^2(s)\Big)\, ds. \tag{9}$$

L denotes the classical curve length (a free variable in our approach), s is the arc-length parameter, and $\Gamma : [0,\, L] \to \Omega$ is a curve with non-vanishing velocity vector. κ is the curvature and α, β are two positively weighted functions, usually related to the image information and which will be defined in Section 4.

Our first step is to cast the elastica energy (9) in the form of path length with respect to a degenerate Finsler metric. For that purpose, let $S^1 = [0, 2\pi[$ be the space of angles, with periodic boundary conditions, and for each angle θ let $\vec{v}_\theta = (\cos\theta, \sin\theta)$ be the corresponding unit vector. For $\gamma = (\Gamma, \theta) \in \Omega \times S^1$ and $\dot\gamma = (\dot\Gamma, \dot\theta) \in \mathbb{R}^2 \times \mathbb{R}$ we define

$$\mathcal{F}^\infty_\gamma(\dot\gamma) := \begin{cases} \|\dot\Gamma\| + |\dot\theta|^2/\|\dot\Gamma\| & \text{if } \dot\Gamma \text{ is positively proportional with } \vec{v}_\theta, \\ \infty & \text{otherwise.} \end{cases} \tag{10}$$

Consider an curve Γ parametrized by arc-length, and its orientation lifting $\gamma = (\Gamma, \theta)$, with $\dot\Gamma(s) := \vec{v}_{\theta(s)}$. By assumption one has $\|\dot\Gamma(s)\| = 1$, hence $\ddot\Gamma(s) = \kappa(s)\dot\Gamma(s)^\perp$, so that $\kappa(s) = \dot\theta(s)$ and

$$\int_0^L (1 + \kappa^2(s))ds = \int_0^L \mathcal{F}^\infty_{\gamma(s)}(\dot\gamma(s))\, ds. \tag{11}$$

The weights α, β of (9) are easily taken into account, by modifying (10) appropriately. Note also that, thanks to the homogeneity of $\mathcal{F}^\infty_\gamma(\cdot)$, the right hand side of (11) is invariant under reparametrizations of the lifted path γ.

The degenerate metric $\mathcal{F}^\infty$ is too singular to apply the fast marching algorithm directly, hence we introduce a family tamings depending on a penalization parameter $\lambda \gg 1$:

$$\mathcal{F}^\lambda_\gamma(\dot\gamma) := \sqrt{\lambda^2\|\dot\Gamma\|^2 + 2\lambda|\dot\theta|^2} - (\lambda - 1)\langle\vec{v}_\theta, \dot\Gamma\rangle. \tag{12}$$

Again, the weights α, β can easily be incorporated into the metric $\mathcal{F}^\lambda$. As $\lambda \to \infty$ one has

$$\begin{aligned} \mathcal{F}^\lambda_\gamma(\dot\gamma) &= \lambda\|\dot\Gamma\|\sqrt{1 + \frac{2|\dot\theta|^2}{\lambda\|\dot\Gamma\|^2}} - (\lambda - 1)\langle\vec{v}_\theta, \dot\Gamma\rangle \\ &= \lambda\|\dot\Gamma\|\Big(1 + \frac{|\dot\theta|^2}{\lambda\|\dot\Gamma\|^2} + \mathcal{O}(\frac{1}{\lambda^2})\Big) - (\lambda - 1)\langle\vec{v}_\theta, \dot\Gamma\rangle \\ &= \|\dot\Gamma\| + \frac{|\dot\theta|^2}{\|\dot\Gamma\|} + (\lambda - 1)(\|\dot\Gamma\| - \langle\vec{v}_\theta, \dot\Gamma\rangle) + \mathcal{O}(\frac{1}{\lambda}), \end{aligned}$$

which tends to $\mathcal{F}^\infty_\gamma(\dot\gamma)$ as $\lambda \to \infty$. The metric $\mathcal{F}^\lambda$ has precisely the required form (6), with a diagonal tensor field $\mathcal{M}$ and a non-zero vector field $\omega(\gamma, \theta) := \vec{v}_\theta$.

The minimal action map $\mathcal{U}^\lambda$ associated to the metric $\mathcal{F}^\lambda$, see (4), can be efficiently computed with the fast marching method [15]. When the penalization parameter λ is sufficiently large, and the spatial and angular resolutions are sufficiently small, it approximates well the limit action map $\mathcal{U}^\infty$ associated to the degenerate metric $\mathcal{F}^\infty$, hence to Euler's elastic energy. In the future, we plan to present a more detailed mathematical convergence analysis. In Section 4, we will give the computational method of the weighted functions α and β shown in (9) by the optimally oriented flux filter [11].

4 Computation of Orientation-lifted Speed

Optimally Oriented Flux: used to extract the local geometry of the image, the oriented flux [11] of an image $I : \Omega \to \mathbb{R}^+$, of dimension $d = 2$, is defined by the amount of the image gradient projected along the orientation $\vec{p}$ flowing out from a 2D circle at point $\hat{x} \in \Omega$ with radius r:

$$f(\hat{x}; r, \vec{p}) = \int_{\partial \mathcal{C}_r} (\nabla (G_\sigma * I)(\hat{x} + r\vec{n}) \cdot \vec{p})(\vec{p} \cdot \vec{n})\, ds, \tag{13}$$

where G_σ is a Gaussian with variance σ and $\vec{n}$ is the outward unit normal vector along $\partial \mathcal{C}_r$. ds is the infinitesimal length on the boundary of $\mathcal{C}_r$. According to the divergence theory, one has

$$f(\hat{x}; r, \vec{p}) = \vec{p}^T \cdot \mathbf{Q}(\hat{x}, r) \cdot \vec{p} \tag{14}$$

for some symmetric matrix $\mathbf{Q}(\hat{x}, r)$ which can be expressed as:

$$\mathbf{Q}(\hat{x}, r) = \begin{pmatrix} \partial_{xx} G & \partial_{xy} G \\ \partial_{yx} G & \partial_{yy} G \end{pmatrix} * \mathbb{1}_r * I(\hat{x}) = \left(\mathbf{F}_r * I\right)(\hat{x}) \tag{15}$$

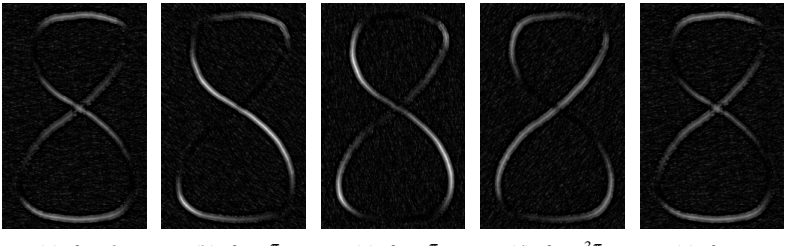

(a) $\theta = 0$ (b) $\theta = \frac{\pi}{4}$ (c) $\theta = \frac{\pi}{2}$ (d) $\theta = \frac{3\pi}{4}$ (e) $\theta = \pi$

Figure 2: Orientation-Lifted Speed with different orientations.

Computation of α and β presented in (9): let $\Lambda_1(\hat{x}, r)$ and $\Lambda_2(\hat{x}, r)$ be the eigenvalues of matrix $\mathbf{Q}(\hat{x}, r)$ and $\Lambda_1(\hat{x}, r) \geq \Lambda_2(\hat{x}, r)$. Assume the grey levels inside the tubular structures are darker than the background so that inside the tubular structure one has $\Lambda_1(\hat{x}, r) \gg 0$ and $\Lambda_2(\hat{x}, r) \approx 0$. Let $r_{max}(\hat{x})$ be the optimal radius of the tubular structure at point $\hat{x}$: $r_{max}(\hat{x}) = \arg\max_r \Lambda_1(\hat{x}, r)$. As shown in [3], the optimally oriented flux (OOF) is a steerable filter with template $\partial_{xx} * \mathbb{1}_r$, which means that we can construct the orientation-lifted function $g : \mathbb{R}^2 \times S^1 \to \mathbb{R}$ as follows:

$$g(\hat{x}, \theta) = \begin{cases} \hat{g}(\hat{x}, \theta) & \text{if } \hat{g}(\hat{x}, \theta) > 0, \\ 0 & \text{otherwise.} \end{cases} \tag{16}$$

$$\hat{g}(\hat{x},\theta) = \left(\vec{u}_\theta^T \mathbf{F}_{r_{max}} \vec{u}_\theta\right) * I(\hat{x}) = \vec{u}_\theta^T \mathbf{Q}(\hat{x}, r_{max}) \vec{u}_\theta, \tag{17}$$

where $\vec{u}_\theta$ is an unit vector associated to $\theta \in S^1$. The function $\alpha : \mathbb{R}^2 \times S^1 \to \mathbb{R}^+$ can be expressed as:

$$\alpha(\hat{x},\theta) = 1 + \mu \frac{g(\hat{x},\theta)}{\|g\|_\infty}. \tag{18}$$

$\alpha(\hat{x},\theta)$ is the speed function which may have a large value when point $\hat{x}$ is inside the vessel and θ follows the exact direction of the vessel at $\hat{x}$. In Fig. 2 we show the function g in different orientations $\theta = \{0, \frac{\pi}{4}, \frac{\pi}{2}, \frac{3\pi}{4}, \pi\}$, in which the high grey level means a large speed value. In this paper, we define

$$\beta = \omega\alpha \quad \text{or} \quad \beta = \eta. \tag{19}$$

where μ, ω and η are three positive constants. μ controls the effects of the speed computed from the images while ω or η control the effects of the curvature penalty.

5 Experiments

Remark 1: in this section, we show some experimental results with comparison to the classical minimal path [8] which we call the *Cohen-Kimmel* model and the isotropic orientation-lifted[1] minimal path model (*orientation-lifted* model) with the metric: $\sqrt{\frac{1}{\alpha^2}(\|\dot{\Gamma}\|^2 + b\|\dot{\theta}\|^2)}$, where $b = 0.1$ in all the experiments. In the following experiments, we use cyan, blue and red lines to represent the extraction results from the *Cohen-Kimmel* model, the *orientation-lifted* model and the proposed model respectively. The blue dots are the end positions while the yellow dots are the initial positions. The green arrows indicate the initial and end directions which also need to be provided in our model. The orientation scale in the following experiments is set to $s_o = \frac{2\pi}{36}$ meaning that we have 36 different directions in the orientation dimension.

Remark 2: We define the optimal orientation map $D : \mathbb{R}^2 \to [0, \pi[$ as:

$$D(\hat{x}) = \arg\max_\theta \{g(\hat{x},\theta)\}. \tag{20}$$

D denotes the orientation or discrete orientation that maximizes the function g; in this way, the user only needs to provide the endpoints of the path in the image, and orientations are determined automatically. However, one still needs to choose between the opposite path directions $D(\hat{x})$ and $D(\hat{x}) + \pi$. We also automatize this step, selecting the path which minimizes the action map $\mathcal{U}^\lambda$, see Fig. 7 for details.

In Fig. 3(a), we show the geodesic path extraction results on the 'U' shape with a short bridge near the bottom of the object. The results of the *Cohen-Kimmel* model and the *orientation-lifted* model prefer to choose a short path though the paths have very large curvature somewhere. In contrast, the proposed model selects a longer but smoother path due to the curvature penalty. In Fig. 3(b), we demonstrate the advantage of using an asymmetric Finsler metric. The two given positions are very close to each other, making the *Cohen-Kimmel* and the *orientation-lifted* models to choose a short way. The proposed model, indicated by the red line, could choose a different path following the initial and end directions

[1] In contrast with the proposed elastica model (10), this model does not require $\dot{\Gamma}$ and v_θ to be collinear.

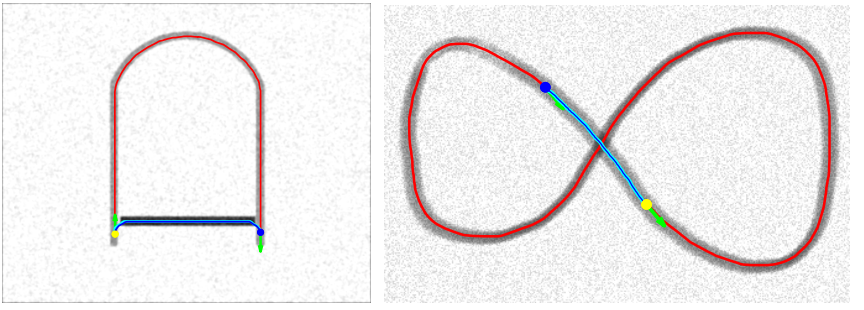

(a) (b)

Figure 3: Comparison results on synthetic images (see text).

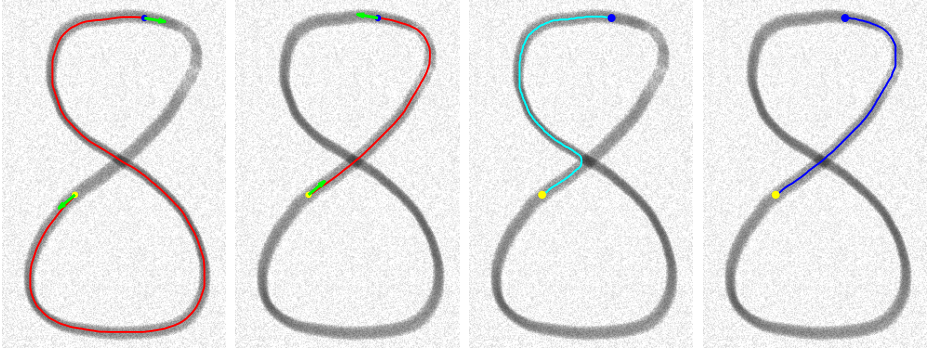

(a) (b) (c) (d)

Figure 4: Comparison results on synthetic images (see text).

(shown as green arrows), though the extracted path has much longer curve length than the results from the *Cohen-Kimmel* and the *orientation-lifted* models.

In Fig. 4(a) and (b), we demonstrate the results of the proposed model with the same given end and initial positions but different directions indicated by the green arrows. It can be seen that the proposed model could choose different paths according to different given directions. Fig. 4(c) and (d) show the results from the *Cohen-Kimmel* and the *orientation-lifted* models.

In Fig. 5, we show the compared results in the patch of a retinal image from the DRIVE dataset [21]. (a) is the original image and (b) is the result from the proposed model. (c) is the *shortcut* result with a small μ defined in (18). (d) is the result from the proposed model with a small curvature penalty ω defined in (19), a path with large curvature. (e) and (f) are the results from the *Cohen-Kimmel* and the *orientation-lifted* models which are similar to (d). In Fig. 6, we demonstrate the results with multi-endpoints and one initial source point. (a) is the result from the proposed model which extracts the desired paths and (b-c) are the results of the *Cohen-Kimmel* and the *orientation-lifted* models respectively, both of which suffer from the *shortcut* problem.

In Fig. 7, we show an initialization method that needs only the initial and end positions to be given. The function D in (20) will provide the optimal directions for each given position.

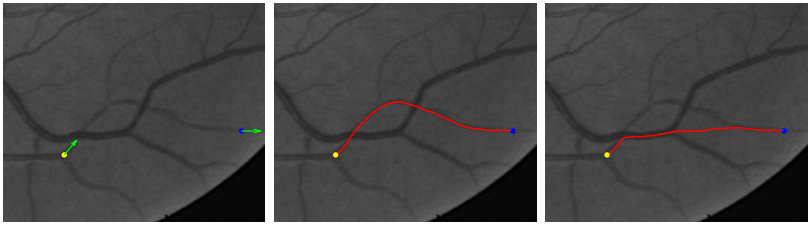

(a) (b) (c)

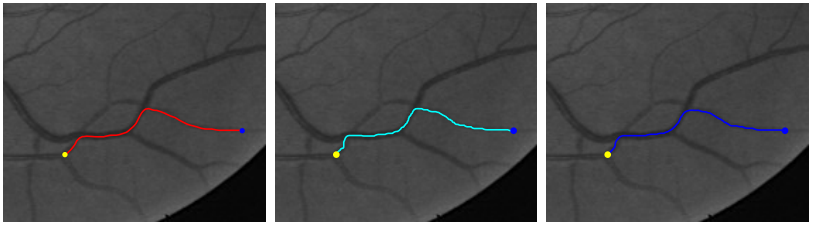

(d) (e) (f)

Figure 5: Extraction results in a retinal image patch (see text).

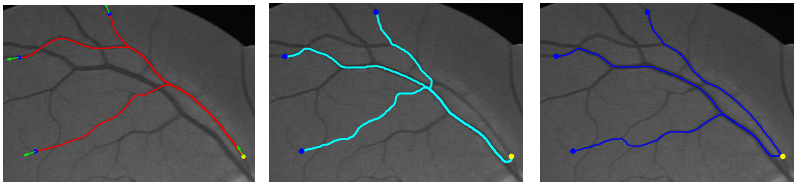

(a) (b) (c)

Figure 6: Extraction results in a retinal image patch (see text).

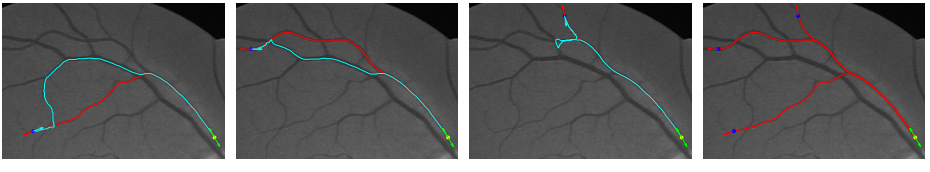

(a) (b) (c) (d)

Figure 7: Extraction results from the proposed model given only initial and end positions (see text).

In Fig. 7(a-c), we show the two obtained paths indicated by cyan and red lines. The cyan arrows indicate the end directions and corresponds to the cyan lines (the same to the red arrows). In (d) we show the final results by removing the paths with larger minimal action map values for each end positions and directions. The blue points are the given end positions and the red arrows are the optimal directions for the corresponding end positions. Yellow points are the given initial positions.

6 Conclusion

In this paper, we show the possibility of incorporating the curvature penalty to the minimal path model via an orientation-lifted Finsler metric and a taming parameter λ. The proposed geodesic energy approximates the weighted Euler's elastica bending energy. Solving the corresponding orientation-lifted Eikonal equation by the state-of-the-art anisotropic fast marching method, our model could determine globally minimizing curves. With the same initial and end positions but different directions, our model could obtain different smooth paths thanks to the asymmetric Finsler metric (Figure 4). When extracted curves are crossing others, our model prefers to choose a smooth path while traditional minimal path models which have removed the second derivative of the curve favour to choose a way with short curve length, especially when the objected curvilinear structure has low grey level contrast (Figures 5 and 6). Experiments show that our model indeed outperforms the traditional models both on synthetic and real images.

In the future we would like to apply the proposed curvature penalized minimal path model to automatically extract the road or vessel network. An interesting research is to combining the keypoints-based minimal path technique and the proposed model for tubular structure network extraction and objects segmentation.

Acknowledgement

The authors would like to thank the suggestions and comments of anonymous reviewers. This work was partially supported by ANR grant NS-LBR, ANR-13-JS01-0003-01.

References

[1] E. J. Bekkers, R. Duits, A. Mashtakov, and G. R. Sanguinetti. Data-Driven Sub-Riemannian Geodesics in SE (2). *Scale Space and Variational Methods in Computer Vision (SSVM 2015)*, pages 613–625, 2015.

[2] F. Benmansour and L. D. Cohen. Fast object segmentation by growing minimal paths from a single point on 2D or 3D images. *Journal of Mathematical Imaging and Vision*, 33(2):209–221, 2009.

[3] F. Benmansour and L. D. Cohen. Tubular Structure Segmentation Based on Minimal Path Method and Anisotropic Enhancement. *International Journal of Computer Vision*, 92(2):192–210, 2011.

[4] D. Chen and L. D. Cohen. Piecewise Geodesics for Vessel Centreline Extraction and Boundary Delineation with Application to Retina Segmentation. *Scale Space and Variational Methods in Computer Vision (SSVM 2015)*, pages 270–281, 2015.

[5] D. Chen, L. D. Cohen, and Jean-Marie Mirebeau. Vessel Extraction using Anisotropic Minimal Paths and Path Score. *IEEE International Conference on Image Processing (ICIP 2014)*, pages 1570–1574, 2014.

[6] L. D. Cohen. On active contour models and balloons. *CVGIP: Image understanding*, 53(2):211–218, 1991.

[7] L. D. Cohen and I. Cohen. Finite-element methods for active contour models and balloons for 2-D and 3-D images. *IEEE Transactions on Pattern Analysis and Machine Intelligence*, 15(11):1131–1147, 1993.

[8] L. D. Cohen and R. Kimmel. Global minimum for active contour models: A minimal path approach. *International Journal of Computer Vision*, 24(1):57–78, 1997.

[9] M. Kass, A. Witkin, and D .Terzopoulos. Snakes: Active contour models. *International Journal of Computer Vision*, 1(4):321–331, 1988.

[10] V. Kaul, A. Yezzi, and Yichang Tsai. Detecting curves with unknown endpoints and arbitrary topology using minimal paths. *IEEE Transactions on Pattern Analysis and Machine Intelligence*, 34(10):1952–1965, 2012.

[11] Max W. K. Law and Albert C. S. Chung. Three Dimensional Curvilinear Structure Detection Using Optimally Oriented Flux. *Computer Vision-ECCV 2008. Springer Berlin Heidelberg*, pages 368–382, 2008.

[12] H. Li and A. Yezzi. Vessels as 4-D curves: Global minimal 4-D paths to extract 3-D tubular surfaces and centrelines. *IEEE Transactions on Medical Imaging*, 26(9):1213–1223, 2007.

[13] J. Melonakos, E. Pichon, S. Angenent, and A. Tannenbaum. Finsler active contours. *IEEE Transactions on Pattern Analysis and Machine Intelligence*, 30(3):412–423, 2008.

[14] Jean-Marie Mirebeau. Anisotropic Fast-marching on Cartesian Grids Using Lattice Basis Reduction. *SIAM Journal on Numerical Analysis*, 52(4):1573–1599, 2014.

[15] Jean-Marie Mirebeau. Efficient fast marching with Finsler metrics. *Numerische Mathematik*, 126(3):515–557, 2014.

[16] David Mumford. Elastica and computer vision. in Algebraic Geometry and Its Applications (C. L. Bajaj, Ed.), Springer-Verlag, New York, pages 491-506, 1994.

[17] M. Péchaud, R. Keriven, and G. Peyré. Extraction of tubular structures over an orientation domain. *IEEE Conference on Computer Vision and Pattern Recognition (CVPR 2009)*, pages 336–342, 2009.

[18] G. Peyré, M. Péchaud, R. Keriven, and L. D. Cohen. Geodesic Methods in Computer Vision and Graphics. *Foundations and Trends in Computer Graphics and Vision*, pages 197–397, 2010.

[19] T. Schoenemann and D. Cremers. Introducing curvature into globally optimal image segmentation: Minimum ratio cycles on product graphs. *IEEE International Conference on Computer Vision (ICCV 2007)*, pages 1–6, 2007.

[20] J. A. Sethian. Fast marching methods. *SIAM Review*, 41(2):199–235, 1999.

[21] J. Staal, M. D Abrámoff, M. Niemeijer, M. A Viergever, and G. Bram. Ridge-based vessel segmentation in color images of the retina. *IEEE Transactions on Medical Imaging*, 23(4):501–509, 2004.

[22] P. Strandmark, J. Ulén, F. Kahl, and L. Grady. Shortest paths with curvature and torsion. *IEEE International Conference on Computer Vision (ICCV 2013)*, pages 2024–2031, 2013.

[23] J. N. Tsitsiklis. Efficient algorithms for globally optimal trajectories. *IEEE Transactions on Automatic Control*, 40(9):1528–1538, 1995.

[24] C. Xu and J. L Prince. Snakes, shapes, and gradient vector flow. *IEEE Transactions on Image Processing*, 7(3):359–369, 1998.